

## Weakly to strongly structured mixtures

M. Kahlweit, R. Strey, and G. Busse

*Max-Planck-Institut für Biophysikalische Chemie, Postfach 2841, D 3400 Göttingen, Germany*

(Received 11 November 1992)

This paper addresses the question as to the differences between weakly and strongly structured mixtures of water ( $A$ ), oils ( $B_k$ ), and nonionic amphiphiles such as alkylpolyglycol ether ( $C_iE_j$ ). Starting with weak short-chain amphiphiles, it is shown that the three-phase body in such mixtures evolves from a tricritical point upon increasing either the carbon number  $k$  of the oil, or the amphiphilicity ( $i, j$ ) of  $C_iE_j$ . In the first case, the three-phase bodies grow monotonically with increasing distance from the tricritical point, with the mixtures, however, remaining weakly structured, whereas in the second case, the three-phase bodies first grow, then pass through maxima in the range of medium-chain amphiphiles, and shrink again as one proceeds to long-chain amphiphiles. In that range in which the three-phase bodies pass their maxima, one observes a gradual evolution of properties that distinguish weakly from strongly structured mixtures. This permits drawing a rather well-defined border line between weakly and strongly structured mixtures in  $(i, j)$ - $k$  space.

PACS number(s): 64.70.—p

## I. INTRODUCTION

Mixtures of water, oils, and amphiphiles form thermodynamically stable colloidal dispersions of either oil domains in water, spongelike bicontinuous structures, or water domains in oil, depending on temperature. With respect to the quantitative description of such “microemulsions,” three models have been hitherto proposed: first, the lattice model, originally proposed by Widom [1] and further developed by Gunn and Dawson [2] and Gompper and Schick [3]; second, the bending-energy model, originally proposed by Jouffroy, Levinson and de Gennes [4] and further developed by Widom [5] and Andelman *et al.* [6]; third, the interfacial tension model, recently proposed by Kahlweit and Reiss [7]. All three models can account for some of the features of microemulsions but not for others which are as important for their macroscopic and microscopic properties. In this paper we shall therefore summarize some of those features that weakly and strongly structured mixtures have in common and some of those that distinguish them from each other. In view of the limited space we shall, however, refrain from discussing which of these features can be described satisfactorily by any of the three models. We shall furthermore restrict our studies to mixtures with nonionic amphiphiles because their phase behavior can be represented exactly in three-dimensional temperature-composition space, whereas mixtures with ionic amphiphiles require the presence of, at least, a fourth component for exhibiting the characteristic features of microemulsions. Some of the experiments were already published in previous papers (see references below), while others are presented for the first time.

## II. PHASE BEHAVIOR

Consider ternary mixtures of a polar protic solvent such as water ( $A$ ), a nonpolar “oil” ( $B$ ) such as an alkane

( $B_k$ ), and a nonionic amphiphile ( $C$ ) such as an alkylpolyglycoether ( $C_iE_j$ ) at atmospheric pressure and normal gravity [8], being represented in an upright phase prism with the Gibbs triangle  $A$ - $B$ - $C$  as the base and  $T$  as the ordinate (Fig. 1). Within a well-defined temperature interval

$$\Delta T \equiv T_u - T_l \quad (2.1)$$

such mixtures separate into three coexisting liquid phases, namely, a water-rich ( $a$ ), an oil-rich ( $b$ ), and an amphiphile-rich phase ( $c$ ). Near the mean temperature

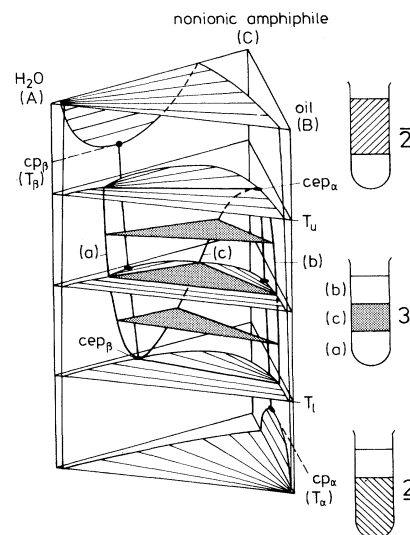


FIG. 1. Phase prism of a water ( $A$ )-oil ( $B$ )-nonionic amphiphile ( $C$ ) mixture. The three test tubes on the right-hand side illustrate how the phases are observed in experiment (schematic).

$$\bar{T} \equiv (T_l + T_u) / 2 \quad (2.2)$$

of  $\Delta T$  one finds a maximum of the efficiency of the amphiphile in homogenizing water and oil, and a minimum of the interfacial tension  $\sigma_{ab}$  between phases *a* and *b*. The separation into three phases is the consequence of the inversion of the distribution of the amphiphile between the two solvents within a narrow temperature range. At ambient *T*, the ternary mixture separates into two phases only, with the amphiphile being more soluble in the (lower) aqueous than in the (upper) oil-rich phase (2). With rising *T*, however, water becomes a poorer solvent for the amphiphile as one deduces from the fact that the binary *A-C* diagram shows an "upper loop" with a (lower) critical point  $cp_\beta$ . The critical line  $cl_\beta$  that starts at  $cp_\beta$ , proceeds into the prism until it terminates at  $T_l$  at the water-rich side of the "central gap." At its end point  $cep_\beta$ , the aqueous phase separates into phases *a* and *c*. Oil, on the other hand, becomes a better solvent for the amphiphile with rising *T* as one deduces from the fact that the binary *B-C* diagram shows a lower miscibility gap with an (upper) critical point  $cp_\alpha$ . With rising *T* phase *c* therefore moves along an ascending trajectory around the binodal surface of the central gap to the oil-rich side, where it merges with phase *b* at  $T_u$  at the end point  $cep_\alpha$  of the critical line  $cl_\alpha$  that enters the phase prism at  $cp_\alpha$ . For  $T > T_u$ , the mixture again separates into two phases only, with the amphiphile now being more soluble in the oil-rich phase than in the aqueous phase (2). The separation into three phases is hence not a particular property of strongly structured mixtures but can also be found in weakly structured mixtures that show a similar temperature dependence of the distribution of a third component between two solvents as, e.g., in *A-B-C* mixtures with weak short-chain amphiphiles.

The minimum of  $\sigma_{ab}$  near  $\bar{T}$  is a necessary consequence of this phase behavior. Because phases *a* and *c*, as well as *b* and *c*, separate at critical end points, the interfacial tension  $\sigma_{ac}$  must rise from zero at  $T_l$ , increasing stronger than linearly with *T* (Fig. 2), whereas  $\sigma_{bc}$  must drop stronger than linearly with *T* to vanish at  $T_u$ . In view of the stability condition

$$0 < \sigma_{ab} \leq \sigma_{ac} + \sigma_{bc} \quad (2.3)$$

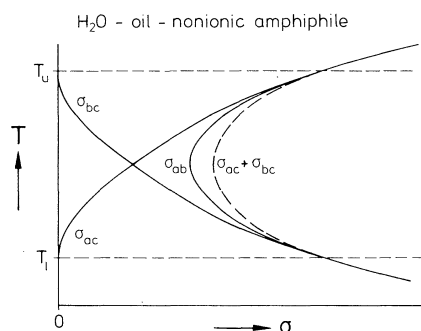


FIG. 2. Temperature dependence of the three interfacial tensions (schematic).

the reverse temperature dependence of  $\sigma_{ac}$  and  $\sigma_{bc}$  must lead to a minimum of  $\sigma_{ab}$  near  $\bar{T}$ . The minimum of  $\sigma_{ab}$  is hence not a particular property of strongly structured mixtures but can also be found in mixtures with weak amphiphiles that show a three-phase body between a lower and an upper critical tie line. The difference between mixtures with weak and strong amphiphiles lies in the absolute magnitude of  $\sigma_{ab}(T = \bar{T})$ . With weak amphiphiles,  $\sigma_{ab}$  is of the order of  $1 \text{ mJ m}^{-2}$ , whereas with strong amphiphiles, it may drop below  $10^{-3} \text{ mJ m}^{-2}$ . We note parenthetically that the minimum of  $\sigma_{ab}$  evolves gradually as one proceeds through the two-phase region from the amphiphile-free *A-B* mixture towards the *a-b* base of the isosceles three-phase triangle (see Fig. 1). Thermodynamics requires for closed systems

$$\left( \frac{\partial \sigma}{\partial T} \right)_{p, n_i, A} = - \left( \frac{\partial S}{\partial A} \right)_{p, n_i, T} \equiv -s^\sigma, \quad (2.4)$$

with *A* denoting the area of the interface. At that *T* near  $\bar{T}$ , at which  $(\partial \sigma / \partial T)$  changes sign, the interfacial excess entropy  $s^\sigma$  per unit area therefore changes sign too, a consequence the physical significance of which remains to be discussed.

Because the separation into three phases arises from the interplay between the two binary gaps *A-C* and *B-C* with the central gap *A-B* both  $T_l$  and  $T_u$  and hence,  $\bar{T}$  are correlated with the temperatures  $T_\beta$  and  $T_\alpha$  of the two critical points  $cp_\beta$  and  $cp_\alpha$ , respectively. Consequently, the dependence of  $\bar{T}$  on the carbon number *k* of the oil, on the carbon number of the hydrocarbon tail, and the number *j* of ethylene oxide groups of the head group of the amphiphile, as well as on additives, can be predicted qualitatively by studying their effect on  $T_\alpha$  and  $T_\beta$ , respectively.

(i) Consider first increasing *k* at fixed *i* and *j* (Fig. 3,

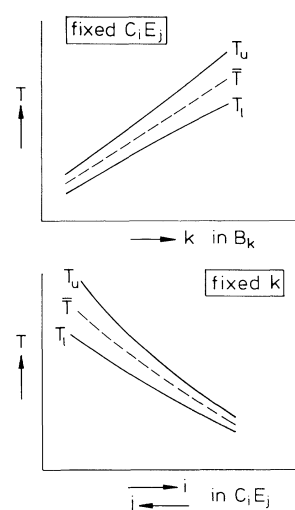


FIG. 3. Dependence of the mean temperature  $\bar{T}$  on the carbon number *k* of the oil at fixed amphiphile (top) and on the strength of the hydrophobic tail (*i*) or that of the hydrophilic head (*j*) of the amphiphile at fixed *k* (bottom, schematic).

top). Increasing  $k$  leaves  $T_\beta$  unaffected, but makes  $T_\alpha$  rise and hence makes  $\bar{T}$  rise (see Fig. 4 in Ref. [9]).

(ii) Consider now changing  $i$  or  $j$  at fixed  $k$  (Fig. 3, bottom). Increasing  $i$  at fixed  $j$  makes both  $T_\alpha$  and  $T_\beta$  drop and hence makes  $\bar{T}$  drop. Increasing  $j$  at fixed  $i$ , on the other hand, makes both  $T_\alpha$  and  $T_\beta$  rise and hence makes  $\bar{T}$  rise (see Fig. 5 in Ref. [9]).

As a rule,  $\Delta T$  widens with rising  $\bar{T}$ , whereas the efficiency of the amphiphile decreases, that is, the mass friction  $\bar{\gamma}$  (see Fig. 6), with

$$\gamma \equiv C / (A + B + C) \quad (2.5)$$

in wt. %, required for homogenizing equal masses of water and oil increases with rising  $\bar{T}$ .

(iii) Consider now adding a salt such as NaCl. Lyotropic salts are much more soluble in the aqueous phase than in the oil-rich phase. Accordingly, it suffices studying their effect on  $T_\beta$ . Because lyotropic ions compete with the head groups of the amphiphile for "free" water molecules in building up their hydration shells, they "salt out" the amphiphile, i.e., make  $T_\beta$  drop, the effect following the order of the "Hofmeister series." Adding a lyotropic salt is thus equivalent to decreasing the effective number  $j$  of ethylene oxide groups of the head (Fig. 3, bottom), which makes  $\bar{T}$  drop. This is demonstrated in Fig. 4, which shows vertical sections through the phase prisms of  $(\text{H}_2\text{O} + \text{NaCl})$ -octane- $\text{C}_{10}\text{E}_j$  ( $j=4,5$ ) mixtures at equal volumes of water and oil. The salt was added to  $\text{H}_2\text{O}$ ; its concentration is expressed as

$$\epsilon = [\text{NaCl}] / ([\text{NaCl}] + [\text{H}_2\text{O}]) \quad (2.6)$$

in wt. %. The fish pattern at elevated temperatures is that of  $\text{C}_{10}\text{E}_5$  with  $\epsilon=0$ . As NaCl is added,  $\bar{T}$  drops, as indicated by the "tails" of the fish, until at  $\epsilon=12.4$  wt. %, the  $\text{C}_{10}\text{E}_5 + \text{NaCl}$  pattern resembles that of the  $\text{C}_{10}\text{E}_4$  fish pattern at  $\epsilon=0$  (dashed line).

(iv) Consider now adding alcohols ( $\text{C}_n\text{E}_0$ ). Their effect on  $\bar{T}$  depends on their carbon number  $n$ . Short-chain alcohols ( $n \leq 3$ ) are more soluble in the aqueous phase than in the oil-rich phase. Accordingly, they distribute mainly between the aqueous phase and the amphiphile-rich phase, thereby increasing their mutual solubility. Adding a short-chain alcohol is thus equivalent to decreasing  $i$ , which makes  $\bar{T}$  rise. Medium- and long-chain alcohols ( $n \geq 4$ ), on the other hand, are more soluble in the oil-rich phase. They distribute mainly between the interfacial layers and the oil-rich phase. Adding a long-chain alcohol is thus equivalent to decreasing  $j$  as well as  $k$ , which makes  $\bar{T}$  drop. At fixed  $(i, j)$  and  $k$ , the effect increases with increasing carbon number  $n$  of the alcohol. This is demonstrated in Fig. 5, which shows vertical sections through the phase tetrahedra of  $\text{H}_2\text{O}$ -octane- $\text{C}_{10}\text{E}_5$ - $\text{C}_n\text{E}_0$  ( $n=4,8$ ) mixtures at 25 °C at equal volumes of water and oil. The fish pattern of the alcohol-free mixture lies at  $\bar{T} \approx 45^\circ\text{C}$  (see Fig. 4). The amount of alcohol that has to be added to lower it to 25 °C as well as the amount of  $\text{C}_{10}\text{E}_5$  required to prepare a homogeneous mixture decreases with increasing  $n$ .

(v) Consider, finally, adding another polar protic solvent such as formamide or glycerol. Their major effect is to change the "opposing forces" between the polar solvent and the tail or head group of the amphiphile, respectively. The effect on the tail can be predicted by comparing the solubility of hydrocarbons in the added solvent with that in water; the effect on the head group can be predicted by taking the dielectric number  $\epsilon_r$  of the added solvent as a crude measure for the strength of its hydrogen bonds. Higher solubility of hydrocarbons is equivalent to decreasing  $i$ , weaker hydrogen bonding to decreasing  $j$ . The two effects may act either in the same or in opposite directions. Formamide ( $\epsilon_r = 109.5$ ), e.g., is apparently a strongly hydrogen-bonding solvent. Howev-

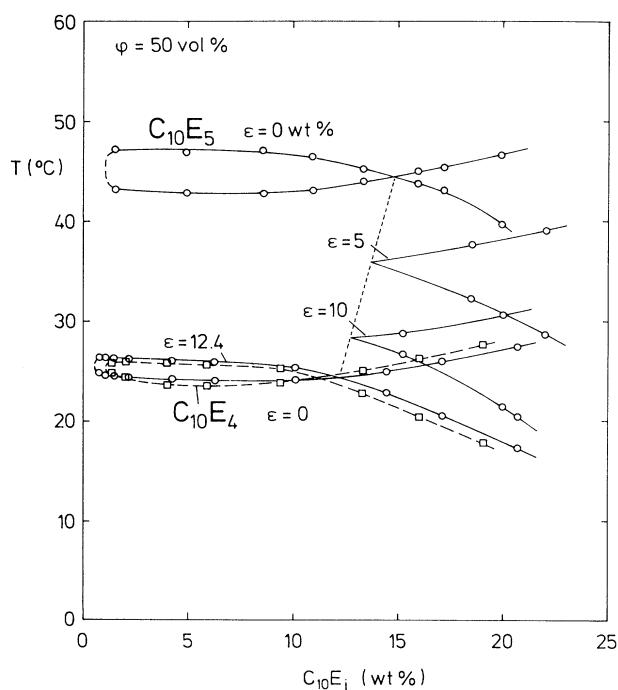


FIG. 4. Lowering the position of the three-phase body of the  $\text{H}_2\text{O}$ -octane- $\text{C}_{10}\text{E}_5$  mixture by adding NaCl, demonstrating that adding a lyotropic salt is equivalent to decreasing  $j$  in  $\text{C}_j\text{E}_j$  [for definition of  $\epsilon$  see Eq. (2.6)].

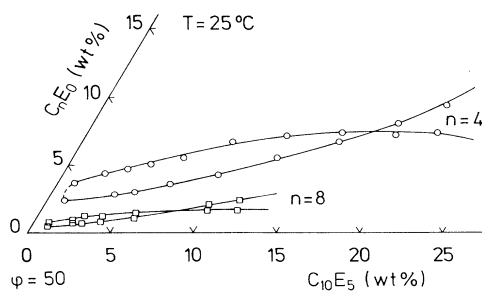


FIG. 5. Lowering the position of the three-phase body of the  $\text{H}_2\text{O}$ -octane- $\text{C}_{10}\text{E}_5$  mixture by adding an alcohol  $\text{C}_n\text{E}_0$  from 45 to 25 °C, demonstrating that the efficiency of the alcohol increases with increasing carbon number  $n$ .

er, because hydrocarbons are considerably more soluble in formamide than in water, adding formamide is equivalent to decreasing  $i$ , that is, it makes  $\bar{T}$  rise [10]. Glycerol ( $\epsilon_r = 42.5$ ), on the other hand, is a poorer solvent for the ethylene oxide groups, and a slightly better solvent for hydrocarbons than water. Adding glycerol is therefore equivalent to decreasing  $j$ , that is, it makes  $\bar{T}$  drop [11].

From this it follows that one may traverse the three-phase interval either by varying temperature or by adding an appropriate fourth component at fixed  $T$ . Consider, for example, the  $\text{H}_2\text{O}$ -octane- $\text{C}_{10}\text{E}_5$  mixture with a three-phase body at  $\bar{T} \approx 45^\circ\text{C}$  (see Fig. 4). At, say,  $35^\circ\text{C}$ , the mixture separates in  $\underline{2}$ . To traverse the three-phase interval, one accordingly has to raise  $T$ . Instead, one may keep  $T$  fixed and add an oil with a lower carbon number  $k$ . Or, if one wants to keep  $k$  fixed, too, add a more hydrophobic amphiphile, that is, increase either  $i$  or decrease  $j$  in  $\text{C}_{10}\text{E}_5$ . Alternatively, one may add a lyotropic salt or an alcohol with  $i \geq 4$ . In all cases, one will find a  $\underline{2} \rightarrow \underline{3} \rightarrow \underline{2}$  transition, with  $\sigma_{ab}$  as well as  $\gamma$  at the binodals first decreasing, then passing a minimum at  $35^\circ\text{C}$ , and increasing again. The fact that this can be achieved by adding substances of very different chemical nature is the consequence of the Gibbs-Duhem relations

$$0 = s \delta T - \delta p + \sum_i c_i \delta \mu_i$$

and (2.7)

$$0 = s^\sigma \delta T + \delta \sigma + \sum_i \Gamma_i \delta \mu_i,$$

which require that the effect of temperature on the chemical potentials in a ternary mixture at fixed mean composition can be replaced by adding an appropriate fourth component at fixed  $T$ .

Qualitatively, the dependence on the phase behavior and of the interfacial tensions on temperature as well as on additives is thus the same for weakly and strongly structured mixtures, which raises the question as to the essential difference between the properties of the two. To find an answer, we have studied the evolution of the three-phase body as well as its properties by proceeding from weak short-chain to strong long-chain amphiphiles, keeping the oil fixed. In our experiments we used  $n$ -octane ( $B_8$ ) as oil, and  $n$ -alkylpolyglycoethers ( $\text{C}_i\text{E}_j$ ) as amphiphiles, proceeding from tertiary butanol ( $t\text{-C}_4\text{E}_0$ ) to  $\text{C}_4\text{E}_1$ ,  $\text{C}_5\text{E}_2$ ,  $\text{C}_6\text{E}_3$ ,  $\text{C}_8\text{E}_4$ ,  $\text{C}_{10}\text{E}_5$ ,  $\text{C}_{12}\text{E}_6$ . This makes  $\bar{T}$  vary very little (see Table I).

### III. EVOLUTION OF THE THREE-PHASE BODY

We start with the weakly amphiphilic tertiary butanol ( $t\text{-C}_4\text{E}_0$ ). Experiment shows that ternary  $\text{H}_2\text{O}$ - $B_k$ - $t\text{-C}_4\text{E}_0$  mixtures separate into three phases for  $k > 10$ , where as for  $k \leq 10$  they separate into two phases only, with a gradual inversion of the distribution of  $t\text{-C}_4\text{E}_0$  between the two solvents [12]. As a consequence, the critical line that enters the phase prism at  $\text{cp}_\alpha$  (see Fig. 1) ascends around the binodal surface from its oil-rich side to its water-rich side with rising  $T$ .

Because the binary  $\text{H}_2\text{O}$ - $t\text{-C}_4\text{E}_0$  mixture does not show an upper loop, the critical line does not terminate at  $\text{cp}_\beta$  but continues to ascend on the water-rich side of the binodal surface. This (connected) critical line can be looked upon as an elastic spring, the bending tension of which can be increased either by adding an oil with a higher carbon number  $k$  at fixed  $(i, j)$  or by adding an amphiphile with a higher  $(i, j)$  at fixed  $k$ . Increasing  $k$  increases the bending tension of the critical line by raising  $\text{cp}_\alpha$ ; increasing  $(i, j)$  increases the bending tension by making the upper  $A$ - $C$  loop appear. The increase of the bending tension manifests itself by the observation that the tangent at its inflection point becomes increasingly horizontal until it eventually breaks at a tricritical point (tcp) (see Fig. 12 in Ref. [8]). A tricritical point is thus a particular plait point at which a homogeneous (quaternary) mixture separates into three instead of two coexisting phases, and as such that point on the binodal surface from which the three-phase body evolves (Fig. 6, top left) to grow into the body of heterogeneous phases with further increasing  $k$  or  $(i, j)$ , respectively (Fig. 6, top right).

The properties of the three-phase body can be characterized by its temperature interval  $\Delta T$ , the height  $h$ , and the base  $l$  of the isosceles triangle (near  $\bar{T}$ ), as well as the interfacial tension  $\sigma_{ab}$  between phases  $a$  and  $b$  connected by that base as a tie line. First, these properties increase monotonically from zero with increasing "distance" from the tcp, irrespectively of whether the distance is increased by increasing  $k$  or  $(i, j)$ . Upon further increasing distance, however, one observes an important difference between the two procedures. If  $k$  is increased at fixed  $(i, j)$ , the above properties continue to increase monotonically, whereas, if  $(i, j)$  is increased at fixed  $k$ ,  $\Delta T$ ,  $h$ , and  $\sigma_{ab}$  first increase, then pass through maxima to decrease again with further increasing  $(i, j)$ . This is demonstrated in Fig. 7, which shows vertical sections through the phase prisms at equal masses of  $\text{H}_2\text{O}$  and oil, with sections through the corresponding three-phase bodies, plotted with the mean temperature  $\bar{T}$  of the bodies as origin of

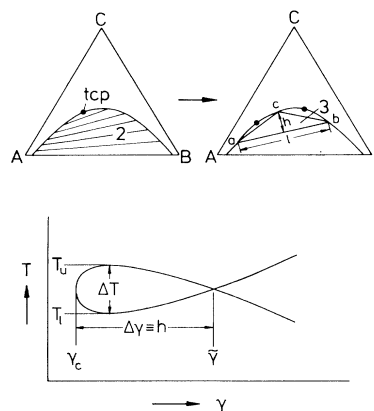


FIG. 6. Evolution of a three-phase body from a tricritical point (top), and its properties as obtained from a vertical section through the phase prism [bottom, schematic; for definition of  $\gamma$  see Eq. (2.5)].

the ordinate. With  $t$ - $C_4E_0$  (Fig. 7, top), the mixture separates into two phases only, with the connected critical line cutting a distinct groove into the body of heterogeneous phases along its trajectory around the binodal

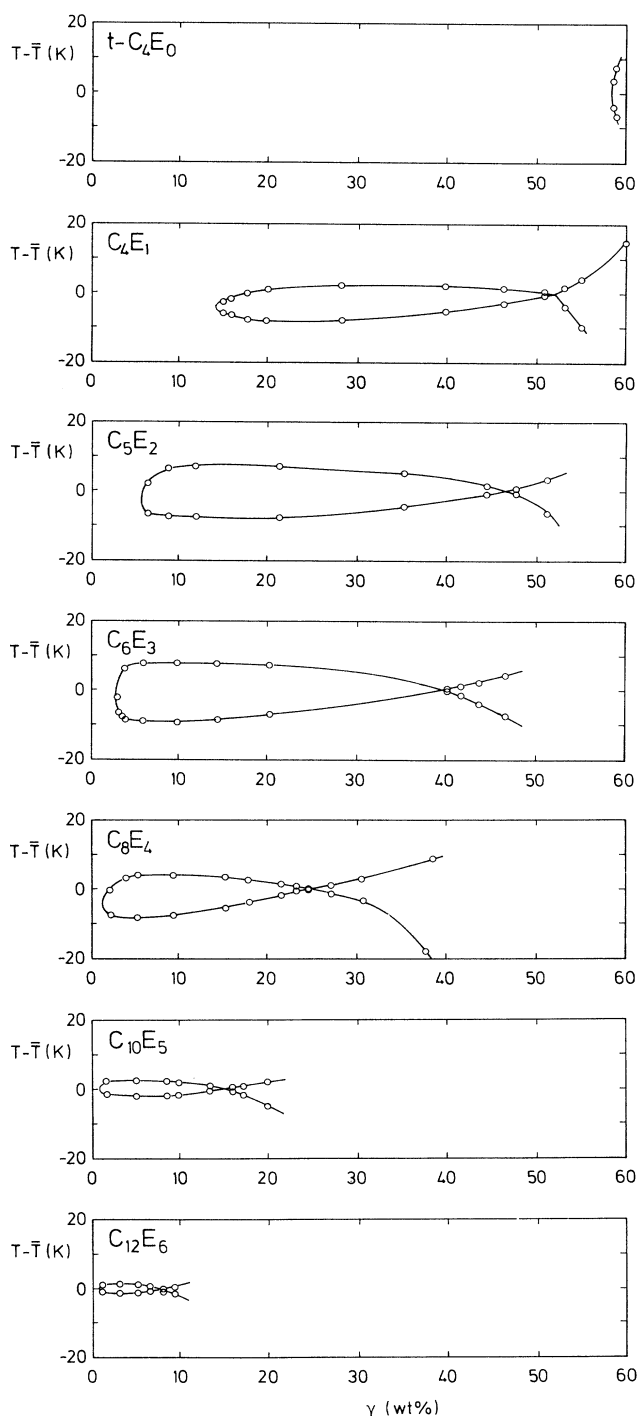


FIG. 7. Evolution of the three-phase bodies of  $H_2O$ -octane- $C_iE_j$  mixtures with  $(i, j)$  increasing from top to bottom, demonstrating that  $\Delta T$  and  $\Delta\gamma$  pass a maximum in the range of medium-chain amphiphiles.

surface. As one proceeds to the more amphiphilic  $C_4E_1$ , the three-phase body is already present at atmospheric pressure from which one deduces that the tcp lies at an amphiphilicity between  $t$ - $C_4E_0$  and  $C_4E_1$ . As one increases  $(i, j)$  further, the fish pattern continues to grow, and to pass through a maximum between  $C_5E_2$  and  $C_6E_3$ . From then on, both the width of the fish pattern (that is,  $\Delta T$ ) and the length of the fish pattern from "head" ( $\gamma_c$ ) to "tail" ( $\bar{\gamma}$ ) shrink,  $\Delta\gamma \equiv (\bar{\gamma} - \gamma_c)$  being a measure for  $h$  (Fig. 6). Simultaneously, the fish pattern moves towards the  $A$ - $B$ - $T$  side of the prism. As the fish pattern grows,  $\gamma_c$  moves rapidly towards the  $A$ - $B$  side with  $\bar{\gamma}$  following only slowly. As the patterns shrink, however,  $\bar{\gamma}$  decreases more rapidly than  $\gamma_c$ . The corresponding data are summarized in Table I.

If this experiment is performed by increasing  $k$  at fixed  $(i, j)$ , one finds  $\Delta T$ ,  $\sigma_{ab}$ ,  $h$ , and  $\bar{\gamma}$  to increase monotonically. This difference is shown schematically in Fig. 8 with  $\Delta T$  vs  $k$  and  $(i, j)$  as rectangular abscissas, and  $\bar{T}$  as origin of the ordinate. Starting from the ternary  $H_2O$ -octane- $t$ - $C_4E_0$  mixture, one may reach a tcp either by increasing  $k$  or  $(i, j)$ . The two tcp's are, evidently, not identical but lie on a tricritical line in  $T$ - $(i, j)$ - $k$  space (dotted). If  $p$  is included as variable, this line shapes a tricritical surface in four-dimensional space.

One may now start at any mixture that lies either in the  $k$  cusp or the  $(i, j)$  cusp, and increase  $(i, j)$  or  $k$ , respectively. In the first case,  $\Delta T$  first widens, then passes a maximum to shrink again, whereas in the second case  $\Delta T$  widens monotonically. This shapes a three-phase body in Fig. 8 that shows a bulge starting at the maximum of the  $(i, j)$  cusp, and moving towards higher  $k$ , though not necessarily parallel to the  $k$  axis. All mixtures lying on the left-hand side of the bulge can be considered as being weakly structured, whereas all mixtures lying on the right-hand side can be considered as being strongly structured. From this it follows that every strongly structured mixture that lies on the right-hand side of the bulge evolves from a tricritical point that (in principle) can be reached by decreasing  $(i, j)$  at fixed  $k$ . In this procedure  $\Delta T$  first widens and then passes a maximum at the bulge before it shrinks to vanish at a tcp that lies on the tricritical line. The most convenient way to perform this experiment is to simply add  $C_2E_0$  [12]. The alternative experiment, namely, decreasing  $k$  at fixed  $(i, j)$ , will only then lead to a tcp, if the initial mixture lies on the left-hand side of the bulge, that is, if it is weakly structured to start with. If it lies on the right-hand side, it will remain strongly structured, with decreasing  $k$  making the three-phase body shrink monotonically until the amphiphilic phase ( $c$ ) is overtaken by the lamellar mesophase. The final stages of this process have not yet been clarified.

The difference between two procedures results from the fact that if  $k$  is increased at fixed low  $(i, j)$ , the amphiphile remains weakly surface active, that is, the interfacial tension  $\sigma_{ab}$  between phases  $a$  and  $b$  remains at the order of  $1 \text{ mJ m}^{-2}$ , whereas, if  $(i, j)$  is increased at fixed  $k$ , this increases the tendency of the amphiphile to adsorb at the water-oil interface, thereby strongly lowering  $\sigma_{ab}$ . This is demonstrated in Fig. 9, which shows  $\sigma_{ab}$  vs  $\gamma$ , measured between the amphiphile-free  $H_2O$ - $B_8$  mixture

TABLE I. H<sub>2</sub>O-*n*-octane-C<sub>*i*</sub>E<sub>*j*</sub> characteristics.

C <sub><i>i</i></sub> E <sub><i>j</i></sub>	T <sub><i>l</i></sub> (°C)	T <sub><i>u</i></sub> (°C)	$\bar{T}$ <sup>a</sup> (°C)	$\Delta T$ <sup>b</sup> (°C)	$\bar{\gamma}$ <sup>c</sup> (wt. %)	$\gamma_c$ (wt. %)	$\Delta\gamma^b$ (wt. %)	$\sigma_{ab}^b$ (mJ m <sup>-2</sup> )
C <sub>4</sub> E <sub>1</sub>	12.9	23.9	18.4	11.0	52.4	14.9	37.5	0.384
C <sub>5</sub> E <sub>2</sub>	25.8	41.1	33.5	15.0	46.6	5.8	40.8	0.360
C <sub>6</sub> E <sub>3</sub>	35.8	53.4	44.6	17.3	39.5	2.9	36.6	0.151
C <sub>8</sub> E <sub>4</sub>	35.5	48.2	41.9	12.5	24.4	1.7	22.7	0.041
C <sub>10</sub> E <sub>5</sub>	42.5	47.1	44.8	4.6	14.7	1.2	13.5	0.013
C <sub>12</sub> E <sub>6</sub>	47.7	49.8	48.8	2.1	7.6	0.7	6.9	0.0034

<sup>a</sup>tcp ≈ 5.<sup>b</sup>tcp = 0.<sup>c</sup>tcp ≈ 58.

( $\sigma_{ab} \approx 50 \text{ mJ m}^{-2}$ ) and the base of the three-phase triangle at  $\bar{T}$ , that is, the head of the fish pattern. With C<sub>4</sub>E<sub>1</sub>,  $\sigma_{ab}$  drops rather smoothly. As (*i, j*) is increased,  $\sigma_{ab}$  drops increasingly steeper, with  $\sigma_{ab}$  at  $\gamma_c$  (at the break of slope) decreasing rapidly (Table I). From this result one deduces that C<sub>4</sub>E<sub>1</sub> must be considered as weak amphiphile. The medium-chain C<sub>5</sub>E<sub>2</sub> and C<sub>6</sub>E<sub>3</sub> lie in the transition range, whereas C<sub>8</sub>E<sub>4</sub> can be considered as an amphiphile with a distinct critical micelle concentration (cmc).

#### IV. CMC SURFACES

In view of Fig. 8 one thus deduces that if *k* is increased at fixed (weak) amphiphilicity, the mixtures remain weakly structured, whereas, if (*i, j*) is increased at fixed *k*, one observes a gradual evolution of structure at amphiphile concentrations above two cmc surfaces that ascend almost vertically within the phase prism. These two cmc surfaces originate from the cmc curves in the two binary A-C and B-C mixtures. The cmc<sup>a</sup> surface starts at the cmc curve of "normal" micelles on the water-rich side of the phase prism, and passes along the corresponding tie lines to the oil-rich side, whereas the cmc<sup>b</sup> surface starts at the cmc curve of "inverse" micelles on the oil-rich side and passes along its tie lines to the water-rich side. Because the energy of formation of normal and inverse micelles differs, in general, the two cmc surfaces do not coincide. Experiment shows that for  $T < \bar{T}$ , the cmc<sup>a</sup> sur-

face lies at lower amphiphile concentrations than the cmc<sup>b</sup> surface (Fig. 10, bottom). With rising *T*, however, the two surfaces approach each other to intersect at  $\bar{T}$  at the *a-b* base of the isosceles three-phase triangle. For  $T > \bar{T}$ , the cmc<sup>b</sup> surface lies at lower amphiphile concentrations than the cmc<sup>a</sup> surface (Fig. 10, top).

At amphiphile concentrations below the lower one of the two cmc surfaces the mixtures are molecularly disperse. However, if for  $T < T_l$  the amphiphile concentration lies above the cmc<sup>a</sup> surface, this leads to the formation of a colloidal dispersion of oil droplets in the aqueous phase (indicated by solid circles in Fig. 10, bot-

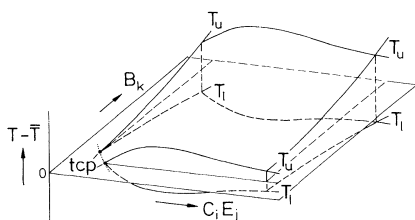


FIG. 8.  $\Delta T$  cusps vs amphiphilicity (*i, j*) at fixed *k*, and carbon number *k* at fixed (*i, j*), respectively, evolving from a tricritical point (tcp). With increasing (*i, j*),  $\Delta T$  passes a maximum to shrink again with further increasing (*i, j*), whereas with increasing *k* it grows monotonically (schematic).

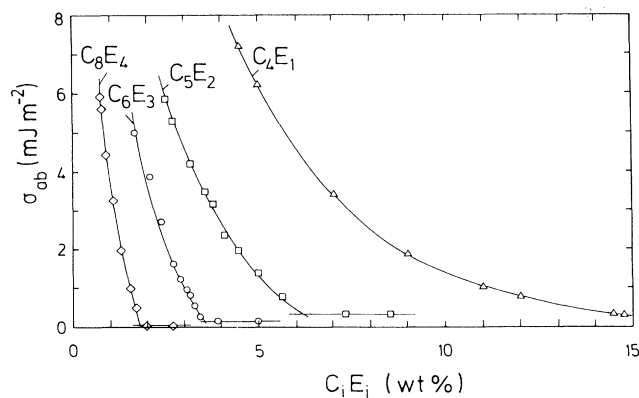
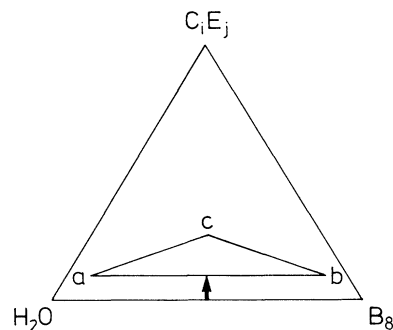


FIG. 9. Adsorption isotherms  $\sigma_{ab}$  vs  $\gamma$  at  $\bar{T}$ , with (*i, j*) as parameter, demonstrating the gradual evolution of a distinct cmc.

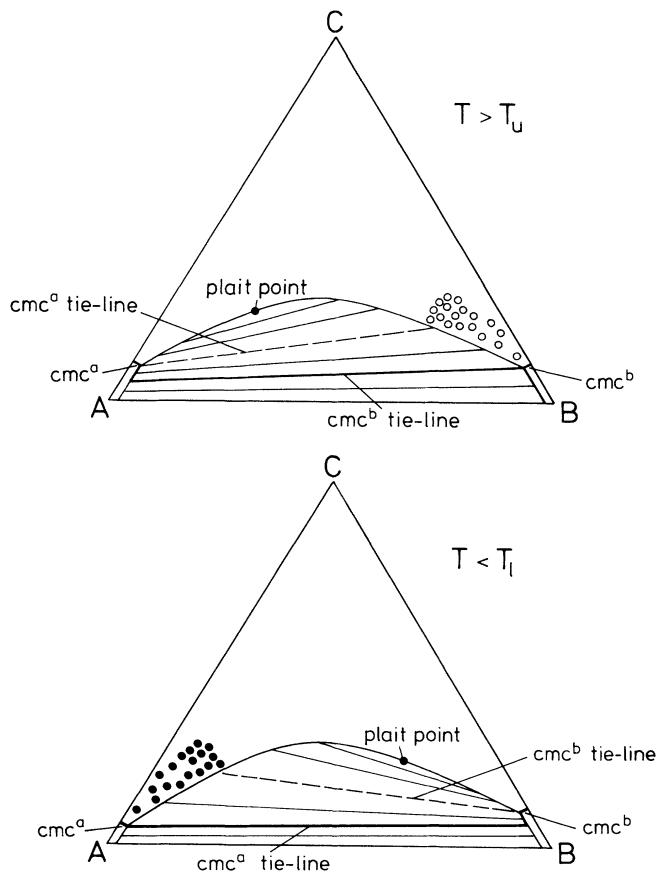


FIG. 10. Isothermal phase diagrams of  $A$ - $B$ - $C$  mixtures at  $T < T_l$  (bottom) and  $T > T_u$  (top). The bold solid line represents the lower of the two cmc tie lines, the dashed line the higher one (schematic). The lower of the two cmc tie lines determines which of the two solvents is dispersed: for  $T < T_l$  oil in water (solid circles), for  $T > T_u$  water in oil (empty circles) dispersions.

tom) in equilibrium with a molecularly disperse oil-rich phase. As one raises  $T$ , this oil in water dispersion separates into a diluted  $a$  and a concentrated dispersion  $c$  at the end point of  $cl_\beta$ . On the other hand, if for  $T > T_u$  the mean amphiphile concentration lies above the  $cmc^b$  surface, this leads to the formation of water droplets in the oil-rich phase (indicated by open circles in Fig. 10, top) in equilibrium with a molecularly disperse aqueous phase. As one lowers  $T$ , this water in oil dispersion separates into phases  $b$  and  $c$  at the end point of  $cl_\alpha$ . Which solvent is dispersed at a certain temperature is thus determined by that one of the two cmc surfaces that lies at the lower amphiphile concentration at that temperature. Figure 11 shows the two cmc surfaces schematically.

Consider now mixtures with distinct cmc surfaces, that is, with phase diagrams as in Fig. 10. Electron micrographs show that along the initial parts of the binodals, the dispersed droplets are isolated and practically monodisperse. Neglecting at this point the thickness of the interfacial layer, one may then set for the volume fraction  $\Phi$  of the dispersed phase

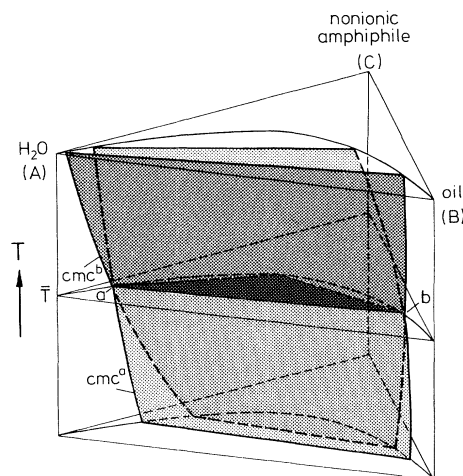


FIG. 11. Phase prism of an  $A$ - $B$ - $C$  mixture with the two cmc surfaces (schematic). For  $T < T_l$ , the  $cmc^a$  surface lies at lower amphiphile concentrations, for  $T > T_u$  it is the  $cmc^b$  surface. At  $T = \bar{T}$ , the two cmc surfaces intersect at the  $a$ - $b$  base of the isosceles three-phase triangle.

$$\Phi = N_v (4\pi/3) r^3 \quad (4.1)$$

and for the interfacial area  $A_v$  per unit volume

$$A_v = N_v 4\pi r^2, \quad (4.2)$$

where  $N_v$  is the number density of the droplets and  $r$  is their mean radius. Elimination of  $N_v$  yields

$$r = 3\Phi / A_v. \quad (4.3)$$

Assuming that at amphiphile concentrations above the cmc tie lines all the excess amphiphile is concentrated in saturated interfacial layers between the droplets and the solvent,  $A_v$  is given by

$$A_v = (\Gamma_s V_c)^{-1} (\Phi_c - \Phi_c^1), \quad (4.4)$$

where  $\Gamma_s$  is the interfacial concentration of the amphiphile  $V_c$  its molar volume,  $\Phi_c$  the total volume fraction of the amphiphile, and  $\Phi_c^1$  that of the monomers dissolved in the two bulk phases (given by  $\Phi_c$  along the corresponding cmc tie line). Equation (4.3) then becomes

$$r = 3\Gamma_s V_c \Phi / (\Phi_c - \Phi_c^1), \quad (4.5)$$

where  $\Gamma_s$  (in curved layers) can be approximated by  $\Gamma_s \approx -(RT)^{-1} (\partial\sigma / \partial \ln\gamma)_{\gamma=\gamma_s}$ , measured at a planar interface (Fig. 9). Experiment now shows that the slopes  $(\Phi_c - \Phi_c^1) / \Phi$  of the binodals become practically constant up to  $\Phi \lesssim 0.3$  as one approaches either  $T_l$  or  $T_u$ , respectively. This is demonstrated in Fig. 12 [13], which shows on bottom the binodals of  $A$ - $B$ - $C$  mixtures on the water-rich side for  $T < T_l$ , and on top those on the oil-rich side for  $T > T_u$ , plotted as  $\Phi$  vs  $(\Phi_c - \Phi_c^1)$ . From this one deduces that along the initial parts of the binodals below  $T_l$  and above  $T_u$  the mean radius of the droplets should depend only weakly on  $\Phi$ , whereas their num-

ber density  $N_v$  should increase linearly with  $\Phi$ . Figure 12 furthermore shows that the slopes of the binodals decrease monotonically as either  $T_l$  is approached from below or  $T_u$  from above. Because experiment shows that  $\Gamma_s$  (measured at planar interfaces) depends only weakly on  $T$ , this implies that the mean radius of the droplets increases upon approaching either one of the critical end-points which, in view of Fig. 2, suggests a relation between  $r$  and  $\sigma_{ab}$  of the type

$$(r^2 \sigma_{ab}) / (k_B T) \approx \text{const.} \quad (4.6)$$

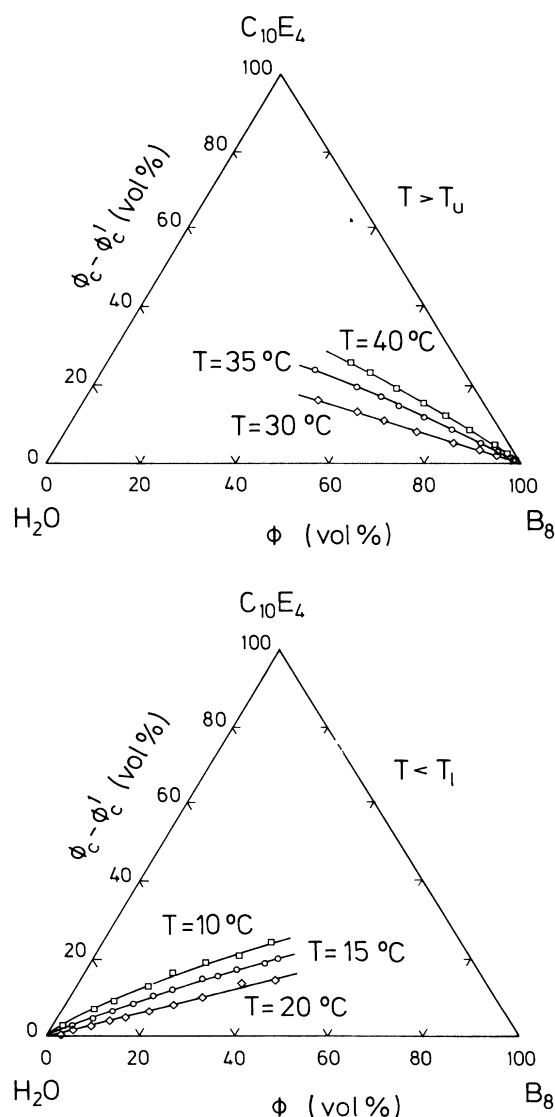


FIG. 12. Binodals in  $\text{H}_2\text{O}$ -octane- $\text{C}_{10}\text{E}_4$  mixtures at various temperatures below  $T_l$  (bottom), and above  $T_u$  (top), demonstrating that the stability limits of the oil in water and water in oil dispersions, respectively, become practically straight upon approaching either  $T_l$  or  $T_u$  [see Eq. (4.5)].

## V. WETTING BEHAVIOR

Widom [14] suggested “seeing the difference (between weakly and strongly structured mixtures) reflected in the wetting vs nonwetting of the oil-water interface by the middle phase” and furthermore predicted for mixtures with nonwetting middle phases “a transition from nonwetting to wetting of the  $a$ - $b$  interface by ( $c$ ) as either one of the two critical end points... is approached.” This suggests studying the wetting behavior of the middle phase as one increases  $(i, j)$  at fixed  $k$ .

Thermodynamic stability of the interfaces between the three coexisting liquid phases  $a$ ,  $b$ , and  $c$  requires each of the three interfacial tensions to be lower than the sum of the other two. This implies for  $\sigma_{ab}$ , in particular,

$$0 < \sigma_{ab} < \sigma_{ac} + \sigma_{bc} . \quad (5.1)$$

If the effect of gravity is reduced by removing the middle phase  $c$  until only a droplet of it is left, this will shape a lens floating at the  $a$ - $b$  interface. Phase  $c$  is then said not to wet the  $a$ - $b$  interface.

If, however, inequality (5.1) does not hold, that is, if

$$0 < \sigma_{ac} + \sigma_{bc} \leq \sigma_{ab} , \quad (5.2)$$

the  $a$ - $b$  interface is unstable, and the system will minimize its free energy by placing a layer of  $c$  between  $a$  and  $b$ . Phase  $c$  is then said to wet the  $a$ - $b$  interface.

Figure 13 [15] shows the contact angles  $\Theta_c$  in  $\text{H}_2\text{O}$ -octane- $\text{C}_i\text{E}_j$  mixtures with  $\text{C}_3\text{E}_2$ ,  $\text{C}_6\text{E}_3$ , and  $\text{C}_8\text{E}_4$  plotted vs  $\vartheta$ , where

$$\vartheta \equiv 2(T - \bar{T}) / \Delta T , \quad -1 \leq \vartheta \leq +1 . \quad (5.3)$$

With a short-chain  $\text{C}_4\text{E}_1$  (not shown in Fig. 13), the middle phase  $c$  wets the  $a$ - $b$  interface in the entire three-phase temperature interval  $\Delta T$ . As one proceeds to the medium-chain  $\text{C}_5\text{E}_2$ , one finds a droplet of  $c$  to contract

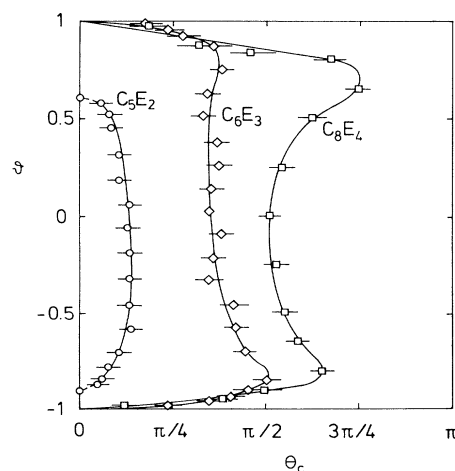


FIG. 13. Temperature dependence of the contact angle  $\Theta_c$  in  $\text{H}_2\text{O}$ -octane- $\text{C}_i\text{E}_j$  mixtures with  $(i, j)$  as parameter. This figure represents the corrected version of Fig. 6 in Ref. [15]. [For definition of  $\vartheta$  see Eq. (5.3)].

to a lens at  $\bar{T}$ , with a contact angle  $\Theta_c < \pi/2$ . However, as either one of the critical endpoints is approached,  $\Theta_c$  decreases monotonically to vanish at some  $T > T_l$  or  $T < T_u$ , respectively. As  $(i, j)$  is increased further,  $\Theta_c(T = \bar{T})$  increases. In addition, one observes a qualitative change in the temperature dependence of  $\Theta_c$ . Upon approaching the critical end points,  $\Theta_c$  does not decrease monotonically, but first increases and then passes through maxima before it drops to zero close to the end-points. Again, what can be achieved by varying  $T$  can also be achieved by adding salt at fixed  $T$  [16].

To discuss the increase of  $\Theta_c(T = \bar{T})$  with increasing  $(i, j)$  one may make use of the relation [17]

$$\cos\Theta_c = [(\sigma_{ab})^2 - (\sigma_{ac})^2 - (\sigma_{bc})^2] / (2\sigma_{ac}\sigma_{bc}) . \quad (5.4)$$

At that  $T$  near  $\bar{T}$ , at which  $\sigma_{ac} = \sigma_{bc}$  (see Fig. 2), this reduces to

$$\cos\Theta_c = \frac{1}{2}(\sigma_{ab}/\sigma_{ac})^2 - 1 , \quad (5.5)$$

where  $\sigma_{ab}/\sigma_{ac} > 1$ . With short-chain amphiphiles, phase  $c$  wets the  $a$ - $b$  interface from which one deduces that, in particular, near  $\bar{T}$

$$\sigma_{ab}/\sigma_{ac} \geq 2 . \quad (5.6)$$

As  $(i, j)$  is gradually increased, there exists one set of  $(i, j)$ —not necessarily integer numbers—at which the lens becomes stable at  $\bar{T}$ , that is, at which  $\cos\Theta_c = 1$ . From Eq. (5.5) it then follows that for this particular amphiphilicity

$$\sigma_{ab}/\sigma_{ac} = 2 . \quad (5.7)$$

We note in parentheses that theory predicts Eq. (5.6) to hold for all near-tricritical mixtures [14]. With further increasing  $(i, j)$ ,  $\cos\Theta_c$  decreases monotonically from which one deduces that the ration  $(\sigma_{ab}/\sigma_{ac})_{T=\bar{T}}$ , too, decreases with increasing  $(i, j)$ . Because  $\sigma_{ab}$  can not drop below  $\sigma_{ac}$ , the contact angle  $\Theta_c(T = \bar{T})$  may thus exceed  $\pi/2$ , but cannot exceed  $2\pi/3$ .

At some higher  $(i, j)$ , the temperature dependence of  $\Theta_c$  changes. To discuss the maximum of  $\Theta_c$  near, e.g.,  $T_l$ , one may make use of the relation [17]

$$0 = \sigma_{ab}\cos\Theta_b + \sigma_{ac}\cos\Theta_c + \sigma_{bc} . \quad (5.8)$$

As one approaches  $T_l$  from above, the two lower phases  $a$  and  $c$  become near-critical. Accordingly, their densities approach each other, whereas the density difference between them and the upper noncritical phase  $b$  remains finite. Sufficiently close to  $T_l$  gravity therefore enforces a practically planar interface between the upper and the two lower phases so that  $\cos\Theta_b \approx -1$ . Equation (5.8) then reduces to

$$\cos\Theta_c \approx (\sigma_{ab} - \sigma_{bc}) / \sigma_{ac} > 0 , \quad (5.9)$$

which ensembles Young's equation. Both  $\sigma_{ab} - \sigma_{bc}$  and  $\sigma_{ac}$  decrease upon approaching  $\text{cep}_\beta$  to vanish at  $T_l$ . Because experiment shows that  $\cos\Theta_c$  first decreases, one deduces that  $\sigma_{ab} - \sigma_{bc}$  first decreases more rapidly than  $\sigma_{ac}$ . Close to  $T_l$ , however,  $\cos\Theta_c$  starts to increase again,

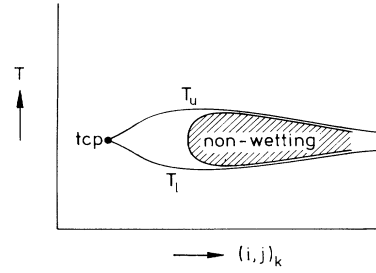


FIG. 14. Nonwetting cusp within the  $\Delta T$ - $(i, j)$  cusp (schematic).

that is, close to  $T_l$   $\sigma_{ac}$  must decrease more strongly than  $\sigma_{ab} - \sigma_{bc}$  so that at some  $T > T_l$ ,  $\cos\Theta_c$  exceeds unity, that is, phase  $c$  starts to spread across the  $a$ - $b$  interface. This nonmonotonic behavior can be explained qualitatively as follows: as long as the compositions of phases  $a$  and  $c$  are sufficiently different, the adsorption of (strong) amphiphiles at the  $a$ - $c$  interface changes only little upon approaching the critical endpoint so that  $\sigma_{ac}$  decreases weakly. However, as the compositions of the two phases become increasingly similar, the driving force for adsorption decreases rapidly until close to  $T_l$ , the final decrease of  $\sigma_{ac}$  resembles that of a weakly structured mixture, being proportional to some power of the density difference between the two phases [18].

The nonwetting cusp is shown schematically in Fig. 14. In near-tricritical weakly structured mixtures, the middle phase  $c$  wets the  $a$ - $b$  interface in the entire  $\Delta T$ . As  $(i, j)$  is gradually increased, phase  $c$  eventually starts contracting to a lens near  $\bar{T}$ , which spreads again upon approaching either one of the two critical end points. With further increasing amphiphilicity, the nonwetting temperature interval widens to (presumably) asymptotically approach the three-phase temperature interval. The apex of the nonwetting cusp lies in that amphiphilicity range at which  $\Delta T$  passes its maximum. Similar to the maxima of  $\Delta T$ , the apex of the nonwetting cusp must not necessarily run parallel to the  $k$  axis.

## VI. SCHREINEMAKERS'S RULE

As can be seen in Fig. 1, the three-phase triangle is surrounded by three two-phase regions of which those adjacent to the  $a$ - $c$  and the  $b$ - $c$  tie lines show plait points that lie on the two branches of the (broken) critical line. At each corner the homogeneous mixture cuts a groove into the body of heterogeneous phases. As it was shown by Schreinemakers in 1913 [19], these grooves are a consequence of thermodynamic stability conditions which require the boundaries between the homogeneous and the two-phase regions to intersect at each corner of the three-phase triangle such that both their extensions pass either into (i) the adjacent two-phase region or (ii) the three-phase triangle. As a consequence, the homogeneous region next to the  $c$  corner of the triangle, in particular, cuts a distinct groove into the body of heterogeneous phases, irrespective of whether the mixture is weakly or strongly structured. Experiment, however, shows that

with short-chain amphiphiles the extensions pass into the adjacent two-phase regions, whereas with long-chain amphiphiles, they pass into the triangle. This is demonstrated in Fig. 15, which shows the grooves at the  $c$  corner of

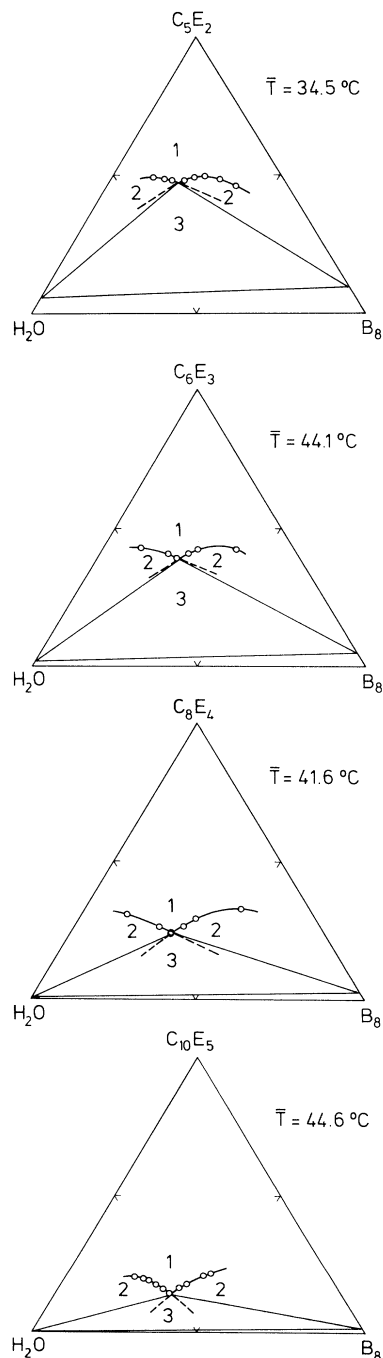


FIG. 15. Extensions of the boundaries of the two-phase regions at the  $c$  corner of the three-phase triangle at  $\bar{T}$  in  $\text{H}_2\text{O}$ -octane- $\text{C}_i\text{E}_j$  mixtures with  $(i, j)$  as parameter, demonstrating the extensions to move gradually from inside the opposite two-phase region into the three-phase triangle with increasing  $(i, j)$ .

the three-phase triangles of  $A$ - $B$ - $\text{C}_i\text{E}_j$  mixtures at  $\bar{T}$ . With  $\text{C}_5\text{E}_2$  (top), the extensions pass clearly into the opposite two-phase regions; with  $\text{C}_{10}\text{E}_5$  (bottom), however, the extensions pass clearly into the triangle. Again, the transition from case (i) to (ii) lies in that amphiphilicity range in which  $\Delta T$  passes its maximum.

At this point one should recall that the experimentally determined three-phase triangles represent the projections of the triple tangent plane to the Gibbs free energy  $G$  at fixed  $T$  and  $p$  onto the base. In general, this tangent plane does not lie parallel to the base (Fig. 16). In the projected three-phase triangle therefore the compositions of the three corners as well as the qualitative behavior of the angles at each corner are correctly reproduced, whereas in general the absolute values of the angles are not. We furthermore remark that from the fact that with short-chain amphiphiles the extensions pass into the opposite two-phase region one should not conclude that this is a property of weakly structured solutions in general. Actually, it can be shown that even in ternary regular mixtures, which must be considered as weakly structured, the extensions may very well pass into the triangle if the interaction parameters are appropriately chosen [20].

## VII. TRAJECTORIES OF THE CRITICAL LINES

Consider now the trajectories of the critical lines that enter the phase prism at  $cp_\beta$  and  $cp_\alpha$ , respectively, to terminate at their critical endpoints at  $T_l$  and  $T_u$ . In 1968, Shinoda and Saito [21] observed that in mixtures with long-chain amphiphiles these critical lines overshoot their end points. That is, the critical line  $cl_\beta$  on the water-rich side descends steeply and passes through a minimum at a temperature below  $T_l$  before it approaches its  $cep_\beta$  from below, whereas the critical line  $cl_\alpha$  on the oil-rich side ascends steeply and passes a maximum at a temperature above  $T_u$  before it approaches its  $cep_\alpha$  from above. This suggests studying the shape of the trajec-

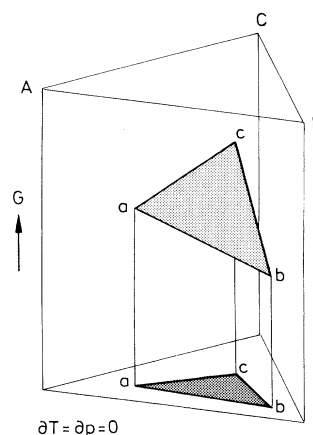


FIG. 16. The experimentally determined three-phase triangle represents the projection of the triangle in the triple tangent plane to the Gibbs free energy onto the base at the corresponding temperature.

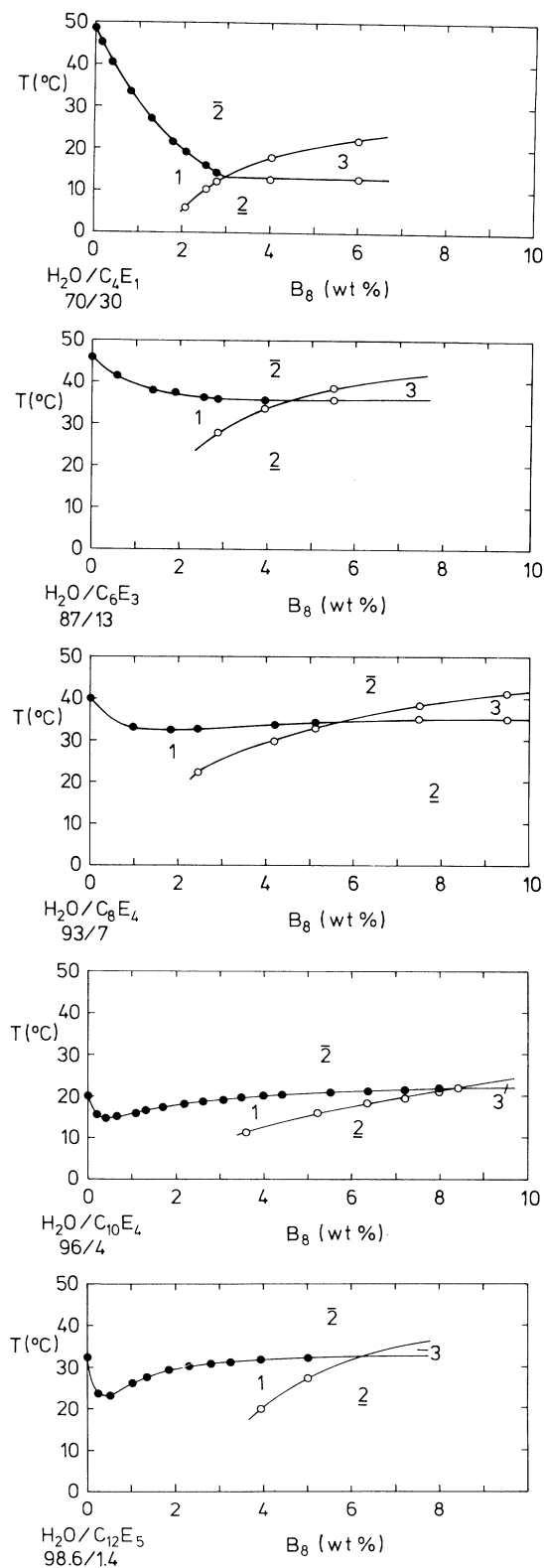


FIG. 17. Vertical sections through the water-rich side of  $\text{H}_2\text{O}$ -octane- $\text{C}_i\text{E}_j$  prisms parallel to their  $A$ - $B$ - $T$  side with  $(i, j)$  as parameter, demonstrating that the critical lines increasingly overshoot their critical end points with increasing  $(i, j)$ .

tories as one proceeds from short- to long-chain amphiphiles at fixed  $k$ . Figure 17 shows vertical sections through the phase prisms of  $A$ - $B_8$ - $\text{C}_i\text{E}_j$  mixtures at fixed amphiphile concentration, that is, in planes parallel to the  $A$ - $B$ - $T$  side of the prism. The amphiphile concentrations chosen correspond to those at the critical points  $cp_\beta$  of the binary  $A$ - $C$  loops. The curve through the full points, though not necessarily identical with the critical lines  $cl_\beta$ , should resemble them rather well. With the short-chain  $\text{C}_4\text{E}_1$  and  $\text{C}_6\text{E}_3$ , the critical lines descend monotonically to their corresponding critical end points, whereas that with  $\text{C}_8\text{E}_4$  is the first to slightly overshoot it. With further increasing amphiphilicity, the minimum becomes increasingly deeper. From this we deduce that the schematic series of isothermal sections through the phase prism as shown, e.g. in Fig. 4 in Ref. [13], holds for weakly structured mixtures only. For strongly structured mixtures it must be replaced by the more realistic though still schematic Fig. 18. At some temperature below  $T_l$ ,  $cl_\beta$  appears with its lowest point (2). With rising  $T$ , this point develops into a loop the tie lines of which run parallel to the  $A$ - $C$  side of the Gibbs triangle (3). With further rising  $T$ , the oil-rich plait point of the loop approaches the central gap to touch it at  $T_l$  as the critical end point of  $cl_\beta$ , which leads to the separation into phases  $a$  and  $c$ . On the oil-rich side, on the other hand, the three-phase triangle disappears at  $T_u$  by separation of a loop from the central gap at the end point of  $cl_\alpha$  (7). With rising  $T$ , this loop shrinks to disappear above  $T_u$  at the maximum of  $cl_\alpha$  (8). Upon isothermal addition of the solute [e.g., oil just below  $T_l$ ; see Fig. 18 (3)], strongly structured mixtures thus first separate into diluted and concentrated dispersions and then become homogeneous again with further increasing solute concentration before they finally expell the solute as molecularly disperse bulk phase.

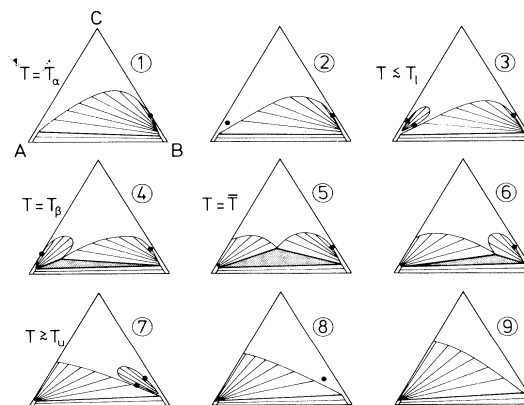


FIG. 18. Evolutions of the three-phase triangle with rising temperatures in  $A$ - $B$ - $C$  mixtures with medium- and long-chain amphiphiles, demonstrating the evolution of isothermal loops adjacent to the central miscibility gap (schematic).

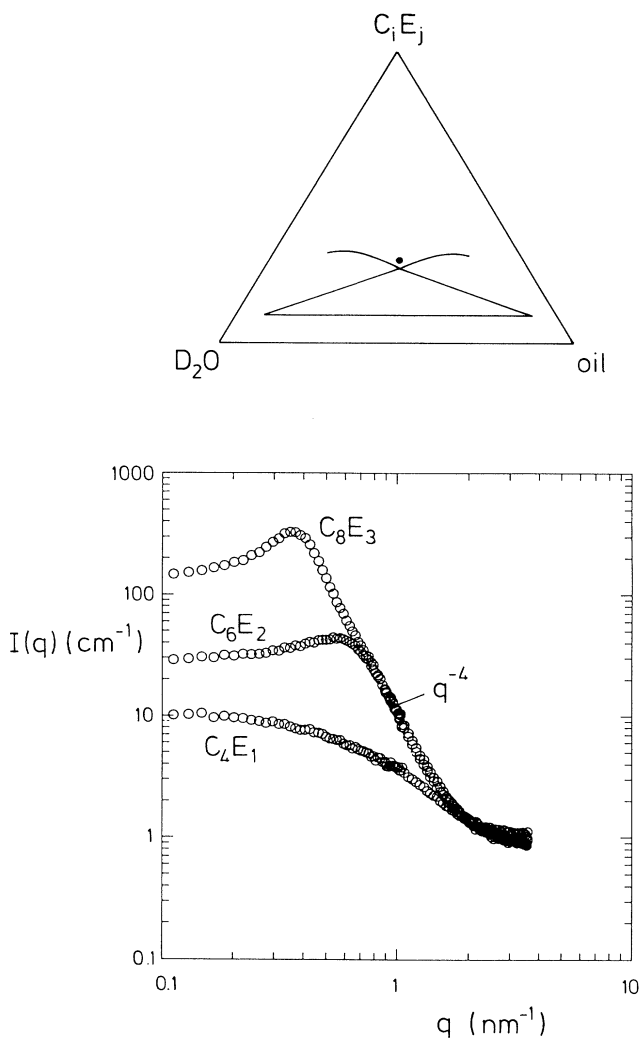


FIG. 19.  $I(q)$  curves in  $D_2O$ -octane- $C_i E_j$  mixtures with  $(i, j)$  as parameter, measured at  $\bar{T}$  in the homogeneous mixture near the  $c$  corner, demonstrating the gradual evolution of a correlation peak with increasing  $(i, j)$ .

### VIII. SMALL-ANGLE NEUTRON SCATTERING

As one increases  $(i, j)$  at fixed  $k$ , small-angle neutron scattering (SANS) experiments show a gradual evolution of a correlation peak in the  $I(q)$  curves, indicating a gradual evolution of a characteristic periodicity  $d$  in strongly structured mixtures [22]. This is demonstrated in Fig. 19 which shows  $I$  vs  $q$  for  $D_2O$ - $B_8$ - $C_i E_j$  mixtures measured at a composition within the groove near corner  $c$ . With the short-chain  $C_4 E_1$ ,  $I(q)$  drops monotonically. Upon

increasing  $(i, j)$  one observes a gradual evolution of a peak followed by an increasingly wider  $q^{-4}$  decay for large  $q$  (Porod's law). The position of the peak moves gradually towards lower  $q$  indicating that  $d$  increases with increasing amphiphilicity, while the fact that Porod's law is increasingly better obeyed indicates that the scattering length density gradient at the interfaces between the domains becomes increasingly steeper. We note that if  $d$  is interpreted as the mean distance between the centers of the domains, the position of the peak is solely determined by the mass balance, irrespective of the model used for describing the mixtures.

### IX. SUMMARY

At fixed pressure, the three-phase bodies in mixtures of  $H_2O$ , oils, and nonionic amphiphiles evolve from a tricritical line that lies in the range of weak short-chain amphiphiles. As a consequence, the phase behavior as well as its dependence on additives such as salts is qualitatively the same for weakly and strongly structured mixtures.

If, at fixed oil, the amphiphilicity is gradually increased, the characteristic properties of the three-phase body first increase monotonically according to the scaling laws for near-tricritical mixtures. In the range of medium-chain amphiphiles, they pass through maxima to decrease again upon further increasing amphiphilicity.

Near the maxima one observes the following: (i) The evolution of two almost vertical cmc surfaces within the phase prism, one defining the cmc of "normal" micelles, the other one that of "inverse" micelles. For  $T < \bar{T}$ , the first lies at lower amphiphile concentrations; for  $T > \bar{T}$ , the second lies at lower amphiphile concentrations. The lower one of the two determines which of the two solvents is dispersed at the corresponding temperature.

(ii) A transition from wetting to nonwetting of the water-oil interface by the amphiphile-rich middle phase.

(iii) The extensions of the boundaries of the two-phase regions adjacent to the three-phase triangle move from inside the opposite two-phase region into the triangle.

(iv) A gradual evolution of isothermal loops adjacent to the central miscibility gap, resulting from the fact that with increasing amphiphilicity the critical lines begin to overshoot their end points.

(v) A gradual evolution of a correlation peak in the  $I(q)$  curves of SANS experiments, indicating a gradual evolution of a characteristic periodicity in the (macroscopically) homogeneous mixtures.

### ACKNOWLEDGMENTS

We are indebted to J. DaCorte, B. Faulhaber, and T. Lieu for their assistance with the experiments.

[1] See, e.g., B. Widom, *J. Chem. Phys.* **84**, 6943 (1986).

[2] J. R. Gunn and K. A. Dawson, *J. Chem. Phys.* **96**, 3152 (1992).

[3] G. Gompper and M. Schick, *Phys. Rev. B* **41**, 9148 (1990).

[4] J. Jouffroy, P. Levinson, and P. G. de Gennes, *J. Phys.*

(Paris) **43**, 1241 (1982).

[5] B. Widom, *J. Chem. Phys.* **81**, 1030 (1984).

[6] D. Andelman, M. E. Cates, R. Roux, and S. A. Safran, *J. Chem. Phys.* **87**, 7229 (1987).

[7] M. Kahlweit and H. Reiss, *Langmuir* **7**, 2928 (1991); M.

- Kahlweit, J. Jen, and G. Busse, *J. Chem. Phys.* **97**, 6917 (1992).
- [8] See, e.g., M. Kahlweit and R. Strey, *Angew. Chem. Int. Ed. Engl.* **24**, 654 (1985).
- [9] M. Kahlweit, R. Strey, and P. Firman, *J. Phys. Chem.* **90**, 671 (1986).
- [10] K. V. Schubert, G. Busse, R. Strey, and M. Kahlweit, *J. Phys. Chem.* **97**, 248 (1993).
- [11] A. Martino and E. W. Kaler, *J. Phys. Chem.* **94**, 1627 (1990).
- [12] M. Kahlweit, R. Strey, M. Aratono, G. Busse, J. Jen, and K. V. Schubert, *J. Chem. Phys.* **95**, 2842 (1991).
- [13] See, e.g., M. Kahlweit, R. Strey, and G. Busse, *J. Phys. Chem.* **94**, 3881 (1990), Fig. 18.
- [14] B. Widom, *Langmuir* **3**, 12 (1987).
- [15] Fig. 13 represents the corrected version of Fig. 6 in M. Aratono and M. Kahlweit, *J. Chem. Phys.* **95**, 8578 (1991); **97**, 5932(E) (1992).
- [16] L. -J. Chen and M. -C. Hsu, *J. Chem. Phys.* **97**, 690 (1992).
- [17] See, e.g., J. S. Rowlinson and B. Widom, *Molecular Theory of Capillarity* (Clarendon, Oxford, 1982), p. 211.
- [18] J. W. Cahn, *J. Chem. Phys.* **66**, 3667 (1977); see also J. Putz, R. Holyst, and M. Schick, *Phys. Rev. A* **46**, 3369 (1992).
- [19] See, e.g., A. Prince, *Alloy Phase Equilibria* (Elsevier, Amsterdam, 1966).
- [20] See, e.g., J. L. Meijering, *Philips Res. Rep.* **6**, 183 (1951), Fig. 21.
- [21] K. Shinoda and H. Saito, *J. Colloid Interface Sci.* **26**, 70 (1968).
- [22] K. V. Schubert and R. Strey, *J. Chem. Phys.* **95**, 8532 (1991).